INSTITUTE OF PHYSICS PUBLISHING JOURNAL OF PHYSICS: CONDENSED MATTER

J. Phys.: Condens. Matter **15** (2003) 2183–2195 PII: S0953-8984(03)57709-8

Intrinsic and extrinsic photoluminescence in the NH_4MnCl_3 cubic perovskite: a spectroscopic study

Ignacio Hernández and Fernando Rodríguez[1]

DCITIMAC, Facultad de Ciencias, Universidad de Cantabria, 39005 Santander, Spain

E-mail: rodriguf@unican.es

Received 24 December 2002
Published 24 March 2003
Online at stacks.iop.org/JPhysCM/15/2183

Abstract

This work investigates the photoluminescence (PL) properties of the cubic chloroperovskite NH_4MnCl_3. Like in most concentrated materials, the Mn^{2+} PL which is located at 2.10 eV at $T = 10$ K strongly depends on the temperature. Optical absorption (OA), emission, and excitation spectroscopy, as well as lifetime measurements, performed on NH_4MnCl_3 indicate that the PL is mainly intrinsic at $T = 10$ K and consists of a broad band located at 2.10 eV. Above this temperature, the PL gradually transforms to extrinsic PL due to exciton migration and subsequent trapping. Further temperature increase above 100 K yields transfer to killers of excitation which are responsible for the PL quenching, and hence the absence of PL at ambient conditions. The exciton traps are identified with perturbed Mn^{2+} sites with the effective activation energy of 52 meV, whilst the activation energy for energy transfer is 47 meV. The existence of these traps has been directly revealed by time-resolved spectroscopy. The detected intrinsic and extrinsic PL bands are displaced by 6 meV, which coincides with the activation energy difference between pure Mn^{2+} and trap Mn^{2+}, as derived from temperature dependence studies of the lifetime $\tau(T)$. Interestingly, a PL band at 1.82 eV is observed above 60 K. This band, which was initially associated with deeper excitation traps, actually corresponds to precipitates of $MnCl_2$ inside NH_4MnCl_3. The correlation analysis performed on NH_4MnCl_3 using OA, PL, and lifetime data provides an estimate of the precipitate concentration of 0.3 mol %. The presence of two separated Mn^{2+} PL bands at different temperatures is a rather common phenomenon in concentrated materials such as $AMnX_3$ (A = NH_4, Rb; X = Cl, F), and has been interpreted in terms of exciton transfer to deeper traps. The present finding stresses the relevance of an adequate structural characterization in dealing with PL in concentrated materials.

[1] Author to whom any correspondence should be addressed.

1. Introduction

The photoluminescence (PL) properties of Mn^{2+} ($3d^5$) in concentrated inorganic compounds depend strongly not only on the local coordination geometry, i.e. the MnX_n complex (X = Cl, Br, F, O; $n = 4, 6, 8$), but also greatly on the structure displayed by the exchange-coupled MnX_n units and the impurity content [1–3]. In isolated Mn^{2+}-doped systems, both the excitation or the optical absorption (OA) and the associated PL rely to a great extent on the crystal field (CF) at the Mn^{2+} site, i.e. the number and nature of the ligands, the local symmetry, and the corresponding bond lengths [4–9]. In concentrated materials, however, the proximity of Mn^{2+} ions favours excitation transfer between nearest Mn^{2+} ions at sites A and B. The exchange interaction between Mn^{2+} ions yields a non-zero probability of transfer of the excitation from A to B: $\tau^{-1}[Mn_A^*\text{–}Mn_B \leftrightarrow Mn_A\text{–}Mn_B^*] \neq 0$ (the Mn^* and Mn refer to the Mn^{2+} electron-excited state and ground state, respectively); the existence of transfer between Mn^{2+} ions favours energy migration within the Mn^{2+} lattice. Consequently, de-excitation does not necessarily take place in the excited Mn^{2+} ion, as in isolated impurities, but can be either in a different Mn^{2+} ion (intrinsic PL), in a perturbed Mn^{2+} trap (extrinsic PL), or in another impurity, which can be either PL (activator) or non-PL (killer). These processes are normally thermally activated and thus depend on the temperature. It must be noted that transfer to excitation killer and killers is the main mechanism for PL quenching in concentrated materials [1, 2]. The knowledge of energy migration processes is crucial for understanding, and eventually improving, the PL properties of concentrated systems. In this way, one-dimensional (1D), two-dimensional (2D), and three-dimensional (3D) systems exhibit different excited-state dynamics, affecting not only the energy-transfer process but also the exciton-trapping mechanism [1, 10]. 3D systems such as $RbMnF_3$ [11, 12] show an efficient energy migration for reaching excitation killer and killers, and therefore PL quenching is expected below room temperature (RT) in 3D materials. $KMnF_3$ [13], $RbMnCl_3$ [14], MnF_2 [15, 16], Cr_2O_3 [17] are examples of non-PL materials at RT. Nevertheless, this behaviour contrasts with the strong PL exhibited by isolated Mn^{2+} ions at RT in isomorphous systems such as Mn^{2+}-doped $KMgF_3$ [5, 6, 18], $RbCaCl_3$ [8, 9], MgF_2 [19], and Cr^{3+}-doped Al_2O_3 [20]. On the other hand, energy transfer to killer and killers of excitation can be substantially reduced in low-dimensional systems [21]. Even though dimensionality reduction from 3D to 2D or 1D may not significantly affect the rate of transfer between Mn^{2+} ions, it strongly influences their PL [22–26]. The present work is devoted to investigating the PL properties of the 3D NH_4MnCl_3 crystal. We select NH_4MnCl_3 ($Pm3m$; $a = 5.050$ Å [27]) because it is, apart from $TlMnCl_3$, the only manganese trichloride with the perovskite structure at ambient conditions [28]. Its structure provides a perfect octahedral symmetry for Mn^{2+} with six corner-sharing octahedra, making it attractive for structural correlation studies. In addition, Mn^{2+} ions are coupled antiferromagnetically with a superexchange Mn–Cl–Mn angle of 180°. Each Mn^{2+} is surrounded by six equivalent Mn^{2+}, which are suitable for energy transfers with identical probabilities. The crystal becomes antiferromagnetic below $T_N = 105$ K [29, 30], and experiences a structural phase transition (PT) from cubic $Pm3m$ to tetragonal $I4/mcm$ at $T = 258$ K [31]. This PT involves rotation of the $MnCl_6^{4-}$ octahedra and reflects the instability of the perovskite structure against pressure or temperature [32, 33]. In general, all perovskite crystals $ABCl_3$ (A and B denote monovalent and divalent metal ions, respectively) undergo a structural PT sequence upon cooling which is mainly associated with the condensation of the R_{25} and M_3 phonon modes. Structurally, these PT mainly involve rotations of the BCl_6 inorganic octahedra around different crystallographic directions [32, 33]. Their non-displacive character in both the chlorides and fluorides ABX_3 (X = Cl, F) keeps the BX_6 units nearly octahedral with similar B–X

distances. An illustrative example of this behaviour is provided by the $KMgCl_3$ crystal whose Mg–Cl distances in the RT orthorhombic *Pnma* structure have values of 2.501, 2.496, and 2.502 Å [35].

The optical properties of NH_4MnCl_3 have been studied previously by OA [36–38] and Raman spectroscopy [39]. The OA spectrum is associated with CF transitions of the Mn^{2+} whose energies are well explained within the $MnCl_6^{4-}$ complex. Exchange effects have also been detected through double-excitation transitions occurring near the crystal absorption threshold using high-pressure spectroscopy [38, 40]. However, PL properties have not so far been investigated, in spite of the ideal structure provided by the NH_4MnCl_3 crystal for establishing structural correlations.

In this work we investigate PL for NH_4MnCl_3 using OA, excitation, and emission spectroscopy techniques, as well as lifetime measurements, as a function of the temperature. The aim is to understand PL processes on the basis of simple models related to thermally activated energy migration. The correlation between the activation energy for exciton detrapping derived from lifetime measurements and time-resolved spectroscopy agrees accurately with the proposed mechanism of migration leading to PL. The results are interpreted in terms of the presence of perturbed Mn^{2+} traps, impurities, and precipitates. Interestingly, we detect PL associated with precipitates of $MnCl_2$ formed in the as-grown crystal. Throughout this work, we stress the relevance of an adequate characterization of both the structure and the impurity content for a proper understanding of PL phenomena in concentrated materials.

2. Experimental details

Single crystals of NH_4MnCl_3 were grown by the Bridgman technique from the melt at 481 °C using stoichiometric amounts of $MnCl_2$ and NH_4Cl (99.9%) [28]. The $Pm3m$ cubic symmetry was checked by x-ray diffraction and the optical quality by means of a polarizing microscope. Parallelepiped single crystals of about $3 \times 3 \times 0.5$ mm^3 were employed. The OA spectra were obtained on a Cary 40 spectrophotometer, whilst the emission and excitation spectra were obtained on an ISA Fluoromax-2 fluorometer. For lifetime measurements and time-resolved spectroscopy, we used an experimental set-up described elsewhere [41]. The analysis of the spectra was performed using the GRAMS32 software package as well as specific programs for instrumental control and analysis developed for this work [41].

3. Results and discussion

3.1. Optical absorption and PL spectra; crystal-field analysis

Figure 1 compares the OA spectra of NH_4MnCl_3 at ambient conditions obtained from single crystals of 0.5 mm thickness and microcrystals. The spectrum in (a) was taken with a conventional spectrophotometer and is very similar to ones reported previously [36–38]. The bands correspond to Mn^{2+} single excitations from the $^6A_{1g}(S)$ ground state to different spin quartet excited states $^4\Gamma_g$ as indicated in figure 1(a) and table 1. The analysis of the transition energies provides values of the Racah parameters: $B = 92$ meV (742 cm^{-1}) and $C = 377$ meV (3042 cm^{-1}), and the ligand-field parameter: $10Dq = 690$ meV (5570 cm^{-1}), that are characteristic of octahedral $MnCl_6^{4-}$ complexes [36–38] according to the perovskite structure of the NH_4MnCl_3 crystal [27]. Interestingly, the use of NH_4MnCl_3 microcrystals (figure 1(b)) enables us to explore the exchange-induced double-excitation bands. The bands observed at 4.86 and 5.25 eV were assigned to the double transitions $^6A_{1g}{}^A(S) + {}^6A_{1g}{}^B(S) \rightarrow$

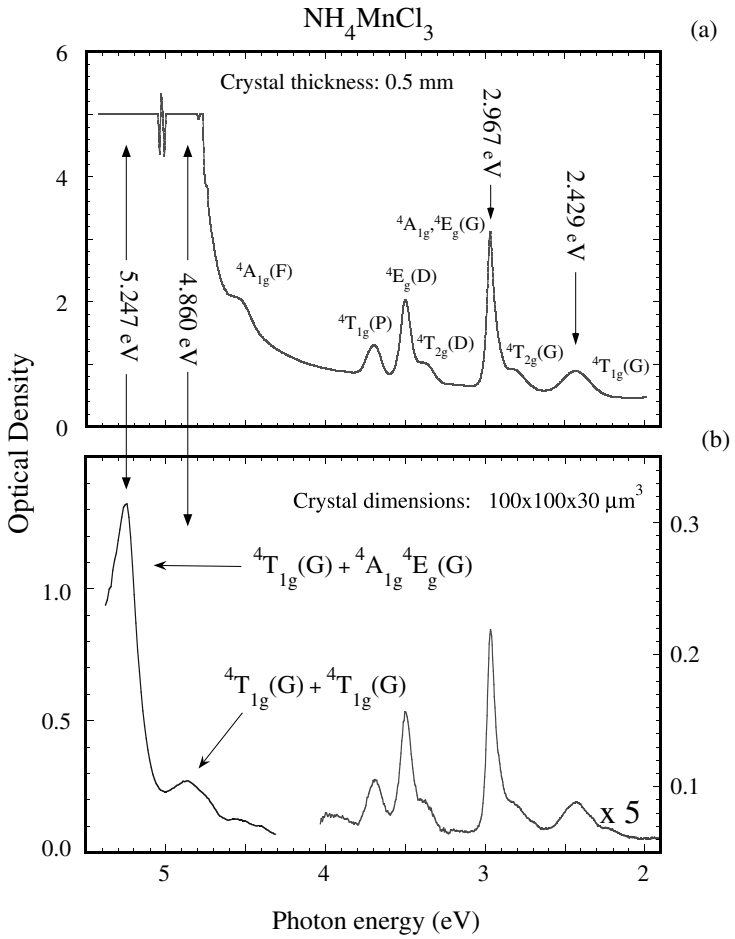

Figure 1. (a) The OA spectrum of the NH_4MnCl_3 perovskite at ambient pressure and RT recorded with a conventional spectrometer. Crystal dimensions: $3 \times 3 \times 0.5$ mm^3. The horizontal line in the UV region indicates the detection limit of the instrument. (b) The OA spectrum of a NH_4MnCl_3 microcrystal ($100 \times 100 \times 30$ μm^3) obtained with an experimental set-up described elsewhere [38]. The bands are identified with the commonly used labels. The energies of the Mn^{2+} single-excitation bands are the same in (a) and (b), but note the resolved UV bands related to double excitations in (b) [38, 40].

$^4T_{1g}{}^A(G) + {}^4T_{1g}{}^B(G)$ and $^6A_{1g}{}^A(S) + {}^6A_{1g}{}^B(S) \rightarrow {}^4T_{1g}{}^A(G) + {}^4A_{1g}$, $^4E_g{}^B(G)$, respectively, using pressure spectroscopy [38, 40].

Although the crystal does not luminescence at RT, it becomes PL upon excitation in any absorption band at low temperature ($T < 110$ K). Figure 2 shows the PL spectrum at $T = 10$ K, and its variation with temperature in the 10–110 K range. The PL spectrum at $T = 10$ K consists of a unique broad band whose maximum is placed at 2.10 eV. Figure 3 shows the variations of the absorption energy and corresponding emission energy together, as functions of the temperature. It must be noted that while the thermal shift undergone by the OA or excitation bands is quite similar [7, 9], the PL band shift is different at low temperatures. In Mn^{2+}-doped systems such as $KMgCl_3$:Mn^{2+} [8], the PL band experiences a continuous blue-shift of 56 meV with increasing temperature in the 10–300 K range. A blue-shift of 14 meV is

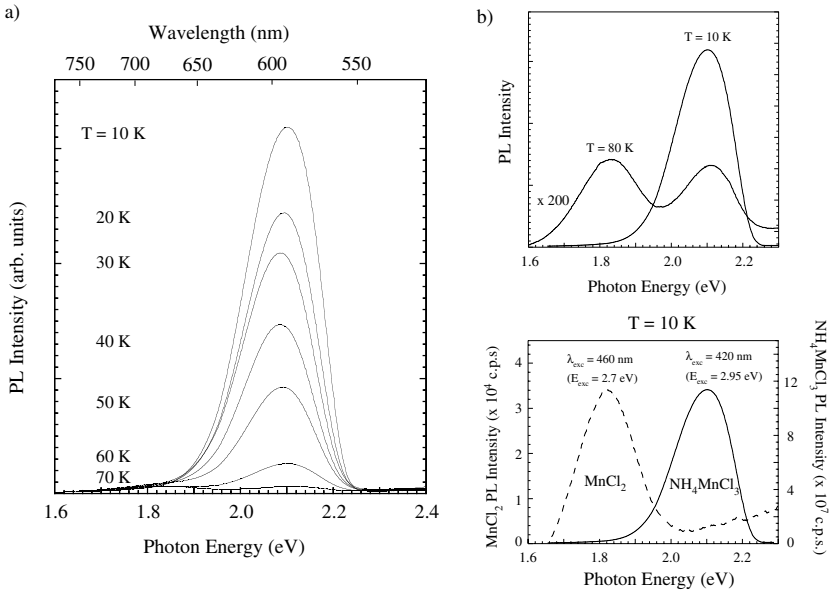

Figure 2. (a) Variation of the PL spectrum of NH_4MnCl_3 with temperature. The PL was induced upon excitation with light of 2.95 eV ($\lambda_{exc} = 420$ nm). In addition to the broad band at 2.10 eV, note the presence of a band at 1.82 eV in the PL spectrum taken at $T = 70$ K. (b) Top: comparison between the PL bands at $T = 10$ and 80 K. Bottom: PL spectra at $T = 10$ K obtained upon excitation at 2.7 eV (460 nm, marked with asterisks in figure 6(a)) and 2.95 eV (420 nm).

Table 1. The experimental photon energy taken at the band maximum and calculated excited-state energies of Mn^{2+} in NH_4MnCl_3. The experimental energies were taken from the OA spectra at $T = 290$ K (figure 1) and 10 K (not shown). The calculated energies (given in parentheses) were obtained from the energy terms of a d^5 electron configuration as a function of the Racah parameters, B and C, and the CF parameter, $10Dq$ [45, 47]. The C/B ratio was obtained from the two $10Dq$-independent $^4A_{1g}$, $^4E_g(G)$ and $^4E_g(D)$ energies, whilst B and $10Dq$ were derived by a fitting using all transition energies. The fit parameters are: $B = 92$ meV (742 cm^{-1}), $C = 377$ meV (3040 cm^{-1}), and $10Dq = 690$ meV (5570 cm^{-1}) for $T = 290$ K; and $B = 97$ meV (784 cm^{-1}), $C = 367$ meV (2960 cm^{-1}), 10Dq = 730 meV (5855 cm^{-1}) for $T = 10$ K. The Trees and seniority parameters for Mn^{2+} were kept fixed: $\alpha = 8.3$ meV (67 cm^{-1}) and $Q = -16.2$ meV (-131 cm^{-1}) [4]. Note that the 5.25 eV band is assigned to the double excitation $^4T_{1g}$ (G) + $^4A_{1g}$, $^4E_g(G)$, rather than $^4T_{1g}(G)$ + $^4T_{2g}(G)$ as would be expected according to the sum of the corresponding single excitations, $E = 5.26$ eV. The proposed assignment was established by pressure spectroscopy [40].

CF band assignment: $^6A_{1g}(S) \rightarrow$	Experimental (calculated) energy (eV) $T = 290$ K	Experimental (calculated) energy (eV) $T = 10$ K
$^4T_{1g}(G)$	2.43 (2.46)	2.41 (2.41)
$^4T_{2g}(G)$	2.83 (2.83)	2.82 (2.82)
$^4A_{1g}(G)$, $^4E_g(G)$	2.97 (2.97)	2.97 (2.97)
$^4T_{2g}(D)$	3.38 (3.35)	3.39 (3.38)
$^4E_g(D)$	3.50 (3.50)	3.52 (3.54)
$^4T_{1g}(P)$	3.70 (3.72)	3.73 (3.73)
$^4T_{1g}(G)$ + $^4T_{1g}(G)$	4.86 (4.92)	(4.82)
$^4T_{1g}(G)$ + $^4T_{2g}(G)$	Not observed [38, 40]	(5.23)
$^4T_{1g}(G)$ + $^4A_{1g}$, $^4E_g(G)$	5.25 (5.43)	(5.38)

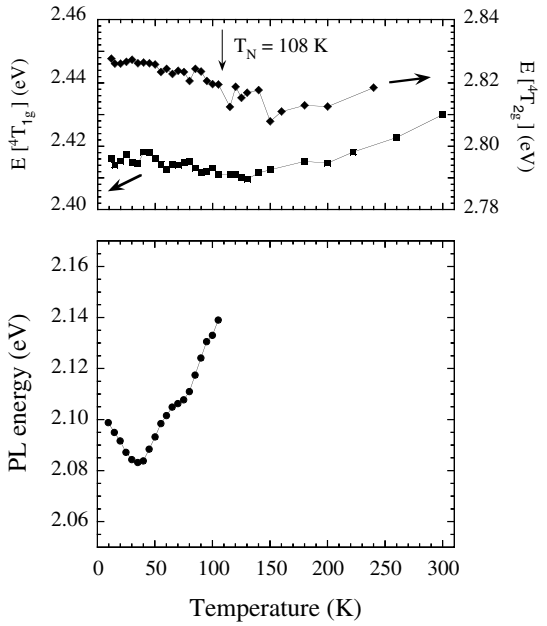

Figure 3. Temperature variation of the energy corresponding to the emission and the first excited-state transition obtained from the PL and OA spectra, respectively. Note that the emission is represented in the 10–110 K range due to the PL quenching at higher temperatures.

also observed for the corresponding first excitation transition $^6A_{1g}(S) \rightarrow {}^4T_{1g}(G)$ in the same temperature range according to expectations from the Tanabe–Sugano diagram for a d^5 ion on the basis of a $10Dq$ reduction. However, an opposite behaviour is observed in concentrated systems such as NH_4MnCl_3 (figures 2 and 3). The PL shifts 15 meV to lower energies in the 10–40 K range. However, a thermal blue-shift of 57 meV takes place upon increasing temperature from $T = 40$ to 100 K. The PL thermal shift shows an anomaly around 70 K that we associate with the presence of a band at 1.82 eV. PL quenching occurs above $T = 100$ K, and is responsible for the absence of PL at ambient conditions.

The red-shifts of 15 and 5 meV experienced by the first and second absorption bands in the 10–120 K (figure 3) contrast with the strong red-shift of 15 meV experienced by the emission band in the 10–40 K range and subsequent blue-shift above 40 K. As well as contributions due to PL from traps, an additional red-shift contribution to the thermal band shift associated with the molecular field at the Mn^{2+} sites in magnetically ordered phases and the PL blue-shift with increasing temperature induced by the low-symmetry CF in the tetragonal $I4/mcm$ phase below $T_C = 258$ K must be considered [1–3, 31–33]. The competition between these two opposite contributions makes a precise analysis of the PL thermal shift difficult in this temperature range. Thus time-resolved spectroscopy can be decisive for elucidating the observed behaviour.

3.2. Time-resolved spectroscopy; excited-state dynamics

The PL time decay, $I(t)$, follows an exponential behaviour at 10 K with an associated lifetime of $\tau = 2.5$ ms. This value is similar to those measured for Rb_2MnCl_4 ($\tau = 3.8$ ms) [42], $CsMnCl_3$ ($\tau = 1.0$ ms), $RbMnCl_3$ ($\tau = 1.1$ ms) [14], but an order of magnitude shorter

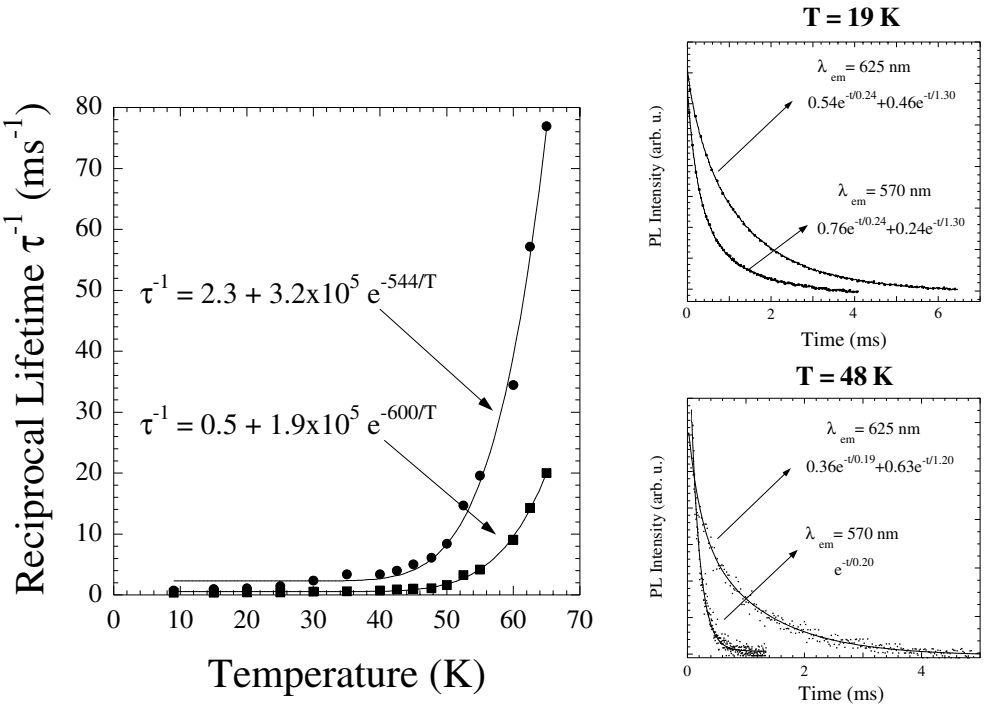

Figure 4. (a) Variations of the PL lifetimes τ_1 and τ_2 with temperature. The two lifetimes correspond to the short and long decay components of $I(t)$. (b) The inset shows the experimental $I(t)$ decay at $T = 19$ and 48 K. The full curves correspond to the least-squares fits of data to the equation $I(E,t) = I_1(E)\exp(-\frac{t}{\tau_1}) + I_2(E)\exp(-\frac{t}{\tau_2})$. The temperature variations of $\tau_1^{-1}(T)$ and $\tau_2^{-1}(T)$ have been fitted to the thermally activated process described by equations (1), (2). The fitted activation energies are $E_e = 47$ meV and $E_a = 52$ meV for $\tau_1(T)$ and $\tau_2(T)$, respectively.

than the lifetimes measured for isolated Mn^{2+} formed in Mn^{2+}-doped $KCaCl_3$ ($\tau = 57$ ms), $CsCaCl_3$ ($\tau = 54$ ms), and $KMgCl_3$ ($\tau = 50$ ms) [9] as a consequence of the higher oscillator strength associated with the PL transition in concentrated materials due to the exchange mechanism [43]. The difference in excited-state behaviour of the isolated Mn^{2+} and the exchange-coupled Mn–Mn is noteworthy.

The PL time decay $I(t)$ in NH_4MnCl_3 cannot be described in terms of one single exponential above 15 K, but an excellent account for $I(t)$ is attained using two single exponentials over the whole temperature range explored. The associated lifetimes τ_1 and τ_2 depend on the temperature, as shown in figure 4. Interestingly, the observed variation is characteristic of exciton migration within the NH_4MnCl_3 crystal. The thermal red-shift observed with increasing temperature above $T = 10$ K is due to PL emission from excitation traps, which are probably related to perturbed Mn^{2+} sites. These Mn^{2+} traps capture the exciton and retain it in a localized low-lying excited state as a consequence of the perturbative CF. The transfer to other neighbouring Mn^{2+} ions is accomplished by thermal activation. This process depends on temperature; hence the associated transfer rate for further migration can be phenomenologically described through the equation [1, 3]

$$\tau^{-1}_{trap\to \mathrm{Mn}} = p\exp\left(-\frac{E_a}{kT}\right) \tag{1}$$

where p is a characteristic frequency for energy transfer depending on the exchange coupling

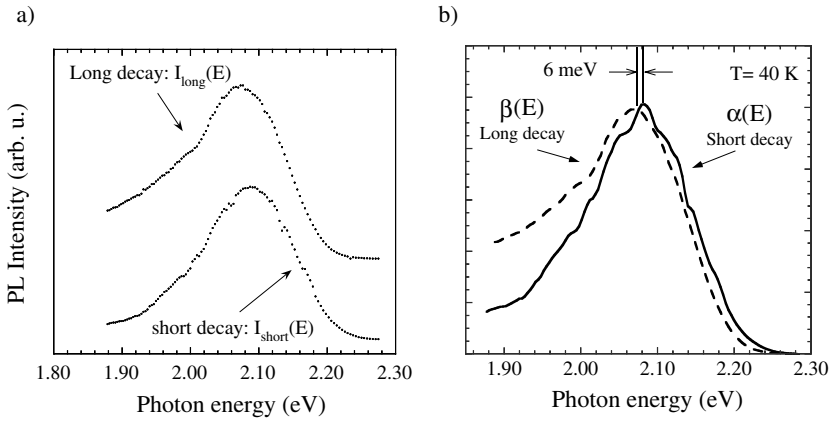

Figure 5. (a) Time-resolved PL spectroscopy corresponding to the short and long decay components of $I(t)$ taken at $T = 40$ K. The PL spectra were taken by means of photon counting after excitation at 2.95 eV. Delay times: 5 and 405 μs; counting times: 180 and 300 μs, for the short and long decay components, respectively. The counting was repeated through 1000 runs for each spectral point. (b) The purely PL bands, denoted by $\alpha(E)$ and $\beta(E)$, were extracted by deconvolution of the time-resolved spectra, $I_{short}(E)$ and $I_{long}(E)$, according to lifetime data of figure 4 using the expressions $I_{short}(E) = A_{11}\alpha(E) + A_{12}\beta(E)$, and $I_{long}(E) = A_{21}\alpha(E) + A_{22}\beta(E)$, with $A_{11} = 1.0$, $A_{21} = 0.0$, and $A_{22} = 0.8$, $A_{12} = 0.2$ at $T = 40$ K. Note that the PL bands $\alpha(E)$ and $\beta(E)$ are shifted by 6 meV.

and the number of Mn^{2+} neighbours, E_a is the activation energy for exciton detrapping, and k is the Boltzmann constant. A similar equation can be quoted for describing rates of transfer from other traps. Therefore, PL emission from one trap results in a red-shift, $\delta = E_a - E_e$, with respect to the pure exciton PL band (intrinsic PL), whose associated Mn–Mn activation energy is E_e. The lifetime is then given by

$$\tau_i^{-1} = \tau_{rad_i}^{-1} + p_i \exp\left(-\frac{E_i}{kT}\right) \tag{2}$$

where E_i is the activation energy for the Mn–Mn ($i = e$) or Mn–Mn trap ($i = a$) detrapping rate at the ith trap, and $\tau_{rad_i}^{-1}$ is the associated PL rate. The curves of figure 4 correspond to the fitting of the data to equation (2) for the pure exciton and an effective single trap. The fitted activation energies for the pure Mn^{2+} and the Mn^{2+} trap are 47 and 52 meV, respectively. Detrapping from Mn^{2+} traps follows energy transfer to killers of excitation and hence PL quenching.

We must stress the presence of a PL band at 1.82 eV above 60 K. Its intensity decreases with increasing temperature and quenches above 100 K. Similar thermally activated red-shifted PL bands were already observed in $RbMnF_3$ and other concentrated materials and conclusively attributed to deeper Mn^{2+} traps yielding well-defined PL bands [12]. Although the PL behaviour of the present band at 1.82 eV is somewhat similar to findings for deeper traps, the observed PL band is in no way associated with Mn^{2+} traps within NH_4MnCl_3 but is associated with $MnCl_2$ precipitates as we show below.

The two different lifetimes involved in the $I(t)$ curves of figure 4 are consistent with PL from purely Mn^{2+} excitons and shallow Mn^{2+} traps. At low temperature, the PL band at 2.10 eV is intrinsic. Upon increasing temperature, detrapping from unperturbed Mn^{2+} results in energy migration and subsequent trapping, thus leading to PL red-shift. Given that exciton capture from traps increases with temperature, a continuous PL red-shift is expected. If we assume that there are only two PL bands (intrinsic and extrinsic) which are shifted by $\delta = E_a - E_e$,

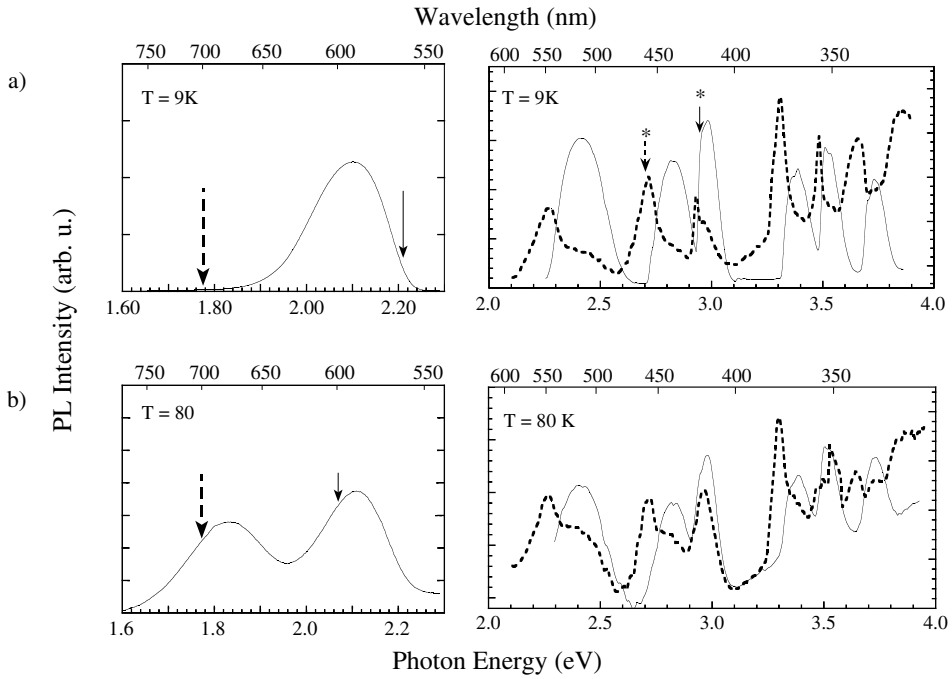

Figure 6. (a) Emission and excitation spectra at $T = 10$ K corresponding to PL bands at 1.82 and 2.10 eV. The excitation spectra were measured at an emission photon energy of 2.21 eV ($\lambda_{em} = 560$ nm; solid arrow and line) and 1.77 eV ($\lambda_{em} = 700$ nm; dotted arrow and line) at $T = 10$ K. (b) Emission and excitation spectra at $T = 80$ K for the same PL bands. The detection was at 2.07 eV ($\lambda_{em} = 600$ nm; solid arrow and line) and 1.77 eV (dotted arrow and line). The excitation spectra, taken at $E_{em} = 2.21$ and 2.07 eV, coincide with those of the NH_4MnCl_3 crystal obtained from OA (figure 1). The excitation energies associated with the emission at $E_{em} = 1.77$ eV are different from those of NH_4MnCl_3 but coincide with the excitation energies of $MnCl_2$ (table 2).

Table 2. Comparison between experimental energies at the band maximum and calculated excited-state energies of Mn^{2+} in NH_4MnCl_3 from the $T = 10$ K excitation spectrum detecting PL at 1.82 eV (figure 6), and in $MnCl_2$ from the $T = 4$ K OA [46]. The fit parameters B, C, and $10Dq$, together with the calculated energies, are also included for comparison purposes. The Trees and seniority parameters for Mn^{2+} were kept fixed: $\alpha = 8.3$ meV (67 cm^{-1}) and $Q = -16.2$ meV (-131 cm^{-1}) [4]. $B = 93$ meV (760 cm^{-1}), $C = 363$ meV (2930 cm^{-1}), and $10Dq = 770$ meV (6250 cm^{-1}).

CF band assignment (O_h notation)	NH_4MnCl_3 (present work) excitations ($E_{em} = 1.82$ eV)	Calculated energies, present work (eV)	$MnCl_2$ OA [44]
$^4T_{1g}(G)$	2.28	2.31	2.29
$^4T_{2g}(G)$	2.72	2.73	2.73
$^4A_{1g}$, $^4E_g(G)$	2.93	2.91	2.93
$^4T_{2g}(D)$	3.31	3.28	3.32
$^4E_g(D)$	3.47	3.45	3.48
$^4T_{1g}(P)$	3.66	3.69	3.78

then the thermal shift from 10 K to high temperature will increase the relative population of Mn^{2+} traps and therefore the PL band will shift continuously from 2.100 to 2.095 eV according to energy migration.

The proposed scenario for exciton migration is confirmed by the fact that the $I(t)$ decay curve measured along the PL band varies with the photon energy. $I(t)$ can be accurately described as a sum of two single exponentials: $I(E,t) = I_1(E)\exp(-\frac{t}{\tau_1}) + I_2(E)\exp(-\frac{t}{\tau_2})$. Whilst lifetimes do not change appreciably along the PL band at a given temperature, the pre-exponential factors do vary significantly. We observe $I_1(E) > I_2(E)$ in the high-energy tail of the PL band, whereas the opposite holds ($I_1(E) < I_2(E)$) in the low-energy tail. This result supports the notion that the PL band consists of two close PL bands arising from non-equivalent Mn^{2+} ions. Figure 5 shows the PL spectrum associated with the long and short decays obtained by time-resolved spectroscopy at $T = 40$ K. At this temperature the emission intensities from the two distinct Mn^{2+} sites are quite similar. Note that the PL spectrum associated with the short lifetime is shifted towards higher energies with respect to the long-lifetime spectrum, thus confirming that we are dealing not with one single PL band but with at least two PL bands. The variation of the time-resolved spectrum with the delay time after excitation allows us to extract the pure PL bands associated with each Mn^{2+} ion, as shown in figure 5. It is worth noting that these two bands, peaking at 2.077 and 2.071 eV, are displaced 6 meV. Furthermore, this shift nearly matches the difference in activation energy between the pure Mn^{2+} and Mn^{2+} trap derived from $\tau^{-1}(T)$: $\delta = E_a - E_e = 5$ meV. Therefore, the present correlation study supports the proposed model for migration on the basis of one single Mn^{2+} trap and killers of excitation.

3.3. Influence of $MnCl_2$ precipitates in NH_4MnCl_3

Figure 6 shows the emission and excitation spectra of NH_4MnCl_3 at $T = 10$ and 80 K. The presence of a PL band at 1.82 eV in the emission spectrum at $T = 80$ K is noteworthy. The band seems to correspond to PL originating from deeper traps. However, its associated excitation spectrum rules out this possibility. Figure 6(b) shows the excitation spectra associated with the PL bands at 2.10 and 1.82 eV at $T = 80$ K. Whereas the former excitation spectrum (solid line) matches the band structure of the OA spectrum of NH_4MnCl_3 (figure 1 and table 1), the latter one (dotted line) is rather different. Its excitation energies coincide with those obtained for single crystals of $MnCl_2$ [44], thus indicating that rather than deeper traps we are actually dealing with $MnCl_2$ precipitates probably formed during the crystal growth. Indeed, this PL at 1.82 eV can also be detected at $T = 10$ K as is shown by the excitation spectrum corresponding to the 1.82 eV emission (figures 2 and 6(a)). Moreover, the difference in energy of the emission bands of NH_4MnCl_3 and $MnCl_2$ basically reflects the variation of the CF at the Mn^{2+} site in these crystals. In fact, the energy difference between the emission bands ($\Delta E_{em} = 0.28$ eV) is partially related to the difference of first excitation energies: $E_{^4T_{1g}}(MnCl_2) - E_{^4T_{1g}}(NH_4MnCl_3) = 0.13$ eV (tables 1 and 2), and agrees with expectations on the basis of the Tanabe–Sugano diagrams [45]. The mismatch energy of 0.15 eV is due to the larger Stokes shift associated with $MnCl_2$ ($\Delta E_S = 0.46$ eV) in comparison to NH_4MnCl_3 ($\Delta E_S = 0.31$ eV). We ascribe this difference to the low-symmetry CF attained at the Mn^{2+} site in $MnCl_2$. The split $^4T_{1g}$ low-lying excited state, which is responsible for the PL at low temperature, is shifted to lower energies by the strong trigonal CF [44], thus providing an additional red-shift contribution to the PL band, with respect to the octahedral symmetry.

A significant feature concerning optical spectroscopy is the possibility of estimating the concentration of $MnCl_2$ precipitates in NH_4MnCl_3. Such a task is difficult to accomplish through standard x-ray diffraction methods due to the low concentration of precipitates. In fact, the estimated Mn^{2+} fraction as $MnCl_2$ precipitates in NH_4MnCl_3 is 0.3 mol%. This estimate is made using OA, excitation, and emission spectra, and lifetime data for both NH_4MnCl_3

and $MnCl_2$. The procedure is as follows. The emission intensities at the PL band maxima (in photons s^{-1}) for NH_4MnCl_3 (band centred at 2.10 eV) and $MnCl_2$ (1.82 eV) upon excitation at 2.95 and 2.70 eV, respectively, are given by

$$\begin{aligned} I_{host}(E_{exc} = 2.95\ \text{eV};\ E_{em} = 2.10\ \text{eV}) &= \frac{N_h}{\tau_h} g_h(2.10\ \text{eV}) \\ I_{prec}(E_{exc} = 2.70\ \text{eV};\ E_{em} = 1.82\ \text{eV}) &= \frac{N_p}{\tau_p} g_p(1.82\ \text{eV}) \end{aligned} \tag{3}$$

where N_h and N_p are the steady-state exciton concentrations in the host and the precipitate, respectively, τ_h and τ_p are the corresponding lifetimes at $T = 10$ K, and $g(E)$ is the spectral factor defined as

$$g(E) = \frac{I(E)\Delta}{\int_{Band} I(E')\,\mathrm{d}E'}. \tag{4}$$

$I(E)$ is the emission band shape and Δ is the monochromator exit slit (in electronvolts). The exciton concentration of equation (3) is proportional to the Mn^{2+} concentration in each phase times the absorption coefficient at the excitation photon energy, $k(E)$:

$$N_h = Ck_h(E) \qquad \text{and} \qquad N_p = Ck_p(E)f \tag{5}$$

where C is an instrumental constant, k_h and k_p are the absorption coefficients of NH_4MnCl_3 and $MnCl_2$ at the excitation energy, 2.95 and 2.70 eV, respectively, and f is the fraction of $MnCl_2$ precipitates. Using equations (3)–(5), we obtain

$$\frac{I_{em}^{MnCl_2}(E_{exc} = 2.70;\ E_{em} = 1.82\ \text{eV})}{I_{em}^{NH_4MnCl_3}(E_{exc} = 2.95;\ E_{em} = 2.10\ \text{eV})} = \frac{N_p}{N_h}\frac{\tau_h}{\tau_p} f = \frac{k_p(2.70)}{k_h(2.95)}\frac{g_p(1.82)}{g_h(2.10)}\frac{\tau_h}{\tau_p} f.$$

Excitation at 2.70 eV (marked with an asterisk in figure 6(a)) provides selective pumping onto $MnCl_2$ precipitates at $T = 10$ K (figure 2(b), bottom), thus improving the method's sensitivity. The emission intensity has been normalized to the excitation intensity throughout this analysis. Taking the measured lifetimes for the 1.82 eV band, $\tau_p \approx 5$ ms, and the 2.10 eV band, $\tau_h \approx 2.5$ ms (figure 4), the absorption coefficients, $k_h(2.95\ \text{eV}) = 2.7\ \text{cm}^{-1}$ (figure 1) and $k_p(2.70\ \text{eV}) = 10.8\ \text{cm}^{-1}$ [46], and the emission spectra of figure 2, we finally get $f = \frac{[MnCl_2]}{[NH_4MnCl_3]} = 0.003$.

This result illustrates the usefulness of correlation spectroscopy for unambiguously detecting $MnCl_2$ precipitates formed inside the NH_4MnCl_3 crystal, and determining its concentration.

4. Conclusions

We have shown that NH_4MnCl_3 exhibits an intrinsic PL at low temperature at 2.10 eV. The exchange-coupled Mn–Mn interaction is responsible for the energy transfer between Mn^{2+} neighbours. Consequently, a thermally activated energy migration is observed with increasing temperature. The emission from shallow traps is mainly accomplished by one perturbed Mn^{2+} centre whose lowest-lying excited state $^4T_{1g}$ is depressed with respect to the exciton level by 6 meV. We demonstrate that further increase of temperature induces trap depopulation, yielding transfer to killers of excitation and subsequent quenching of PL at ambient conditions. A PL band which is observed at 1.82 eV during the PL quenching process has been attributed to PL coming from neither deeper Mn^{2+} traps in NH_4MnCl_3 nor impurities, but from $MnCl_2$ precipitates formed inside the NH_4MnCl_3 bulk. Furthermore, time-resolved emission and excitation spectroscopy allows us to distinguish intrinsic, extrinsic, and outer PL within NH_4MnCl_3. The comparison of the activation energy obtained from lifetime data and the shifts

of the respective PL bands from time-resolved spectroscopy provides direct confirmation of the proposed exciton-trapping model.

Acknowledgments

We thank Professor Güdel for fruitful discussions and collaboration. Financial support from the Spanish MCyT (Project No BFM2001-0695) is acknowledged. One of the authors (IH) thanks the Ministerio de Educación, Cultura y Deporte for an FPU grant (AP2001-1680).

References

[1] Di Bartolo B 1978 *Luminescence of Inorganic Solids* (New York: Plenum)
[2] Lever A B P 1984 *Inorganic Electronic Spectroscopy* (New York: Elsevier)
[3] Henderson B and Imbusch G F 1989 *Optical Spectroscopy of Inorganic Solids* (New York: Oxford University Press)
[4] Rodríguez F and Moreno M 1986 *J. Chem. Phys.* **84** 692
[5] Rodríguez F, Riesen H and Güdel H U 1991 *J. Lumin.* **50** 101
[6] Marco de Lucas M C, Rodríguez F and Moreno M 1994 *Phys. Rev.* B **50** 2760
[7] Marco de Lucas M C, Rodríguez F and Moreno M 1995 *J. Phys.: Condens. Matter* **7** 7535
[8] Marco de Lucas M C, Rodríguez F, Prieto C, Verdaguer M, Moreno M and Güdel H U 1995 *Radiat. Eff. Defects Solids* **135** 95
[9] Marco de Lucas M C, Rodríguez F, Güdel H U and Furrer N 1994 *J. Lumin.* **60/61** 581
[10] Blasse G 1980 *Luminescence and Energy Transfer, Structures and Bonding* (Berlin: Springer)
[11] Wunsch F R and Gebhardt W 1989 *J. Phys.: Condens. Matter* **1** 855
[12] Di Bartolo B, Danko J and Pacheco D 1987 *Phys. Rev.* B **35** 6386
[13] Goldberg V, Pacheco D, Moncorge R and Di Bartolo B 1979 *J. Lumin.* **18/19** 143
[14] Kambli U and Güdel H U 1984 *J. Phys. C: Solid State Phys.* **17** 4041
[15] Flaherty J M and Di Bartolo B 1973 *Phys. Rev.* B **8** 5232
[16] El Kadiri M, Baruchel J, Rodríguez F, Moreno M and Henry J Y 1986 *J. Magn. Magn. Mater.* **54–57** 853
[17] McClure D S 1963 *J. Chem. Phys.* **38** 2289
[18] Rodríguez F, Moreno M, Tressaud A and Chaminade J P 1987 *Cryst. Lattice Defects Amorph. Matter* **16** 221
[19] Suzuki Y, Sibley W A, El-Bayoumi O H, Roberts T M and Bendow B 1987 *Phys. Rev.* B **35** 4472
[20] Maiman T 1960 *Nature* **187** 493
[21] McPherson G L, Devaney K O, Willard S C and Francis A H 1979 *Chem. Phys. Lett.* **68** 9
[22] Morita M and Kameyama M 1981 *J. Lumin.* **24/25** 79
[23] Day P, Ingletto G, Low T, Norris J O R and Stewart B 1985 *J. Chem. Soc. Faraday Trans.* II **81** 1201
[24] Tsuboi T, Matsubara A, Kato K, Iio K and Henderson B 1995 *Phys. Status Solidi* b **188** K35
[25] Auerbach R A and McPherson G L 1986 *Phys. Rev.* B **33** 6815
[26] Knochenmuss R and Güdel H U 1987 *J. Chem. Phys.* **86** 1104
[27] Tornero J D, Cano F H, Fayos J and Martínez-Ripoll M 1978 *Ferroelectrics* **78** 123
[28] Marco de Lucas M C, Rodríguez F, Prieto C, Verdaguer M and Güdel H 1995 *J. Phys. Chem. Solids* **56** 995
[29] Shachar G, Makovsky J and Shaked H 1971 *Solid State Commun.* **9** 493
[30] Tornero J D, López F J and Cabrera J M 1975 *Solid State Commun.* **16** 53
[31] Pique C, Palacios E, Burriel R, Rubín J, González D, Navarro R and Bartolomé J 1990 *Ferroelectrics* **109** 27
[32] Vaills Y, Buzaré J Y, Gibaud A and Launay C 1986 *Solid State Commun.* **60** 139
[33] Fujii Y, Hoshino S, Yamada Y and Shirane G 1974 *Phys. Rev.* B **9** 4549
Glaser A M 1975 *Acta Crystallogr.* A **31** 756
[34] Lehner N, Rauh H, Strobel K, Geick R, Heger G, Bouillot J, Renker B, Rousseau M and Stirling W G 1982 *J. Phys. C: Solid State Phys.* **15** 6545
[35] Brynestad J, Yakel H L and Smith G P 1966 *J. Chem. Phys.* **45** 4652
[36] Agulló-Rueda F, Calleja J M, Jaque F, Tornero J D and Palacio F 1986 *Solid State Commun.* **60** 331
[37] Hernández D, Rodríguez F, Moreno M and Güdel H U 1999 *Physica* B **265** 186
[38] Rodríguez F, Hernández D and Güdel H U 1999 *Phys. Rev.* B **60** 10598
[39] Agulló-Rueda F, Calleja J M and Tornero J D 1987 *Solid State Commun.* **62** 551
[40] Rodríguez F, Hernández D and Güdel H U 2000 *Sci. Technol. High Pressure* **2** 987
[41] Hernández I 2002 *Graduate Thesis* University of Cantabria

[42] Tsuboi T and Iio K 1993 *Phys. Status Solidi* b **179** K47
[43] Ferguson J, Guggenheim H J and Tanabe Y 1966 *J. Phys. Soc. Japan* **21** 692
[44] Pollini I, Spinolo G and Benedek G 1980 *Phys. Rev.* B **22** 6369
[45] Sugano S, Tanabe Y and Kamimura H 1970 *Multiplets of Transition-Metal Ions* (New York: Academic)
[46] Regise M and Farge Y 1976 *J. Physique* **37** 627
[47] Griffith J S 1980 *The Theory of Transition-Metal Ions* (Cambridge: Cambridge University Press)